Fine-mapping and functional studies highlight potential causal variants for rheumatoid arthritis and type 1 diabetes

Harm-Jan Westra[1,2,3,4,5,20], Marta Martínez-Bonet [4,20], Suna Onengut-Gumuscu [6,7], Annette Lee[8], Yang Luo[1,2,3,4], Nikola Teslovich[1,2,3,4], Jane Worthington[9,10], Javier Martin[11], Tom Huizinga[12], Lars Klareskog[13], Solbritt Rantapaa-Dahlqvist[14], Wei-Min Chen[6,7], Aaron Quinlan [6,15,16], John A. Todd[17], Steve Eyre[9,10], Peter A. Nigrovic[4,18], Peter K. Gregersen[8], Stephen S. Rich[6,7] and Soumya Raychaudhuri [1,2,3,4,9,19]*

To define potentially causal variants for autoimmune disease, we fine-mapped[1,2] 76 rheumatoid arthritis (11,475 cases, 15,870 controls)[3] and type 1 diabetes loci (9,334 cases, 11,111 controls)[4]. After sequencing 799 1-kilobase regulatory (H3K4me3) regions within these loci in 568 individuals, we observed accurate imputation for 89% of common variants. We defined credible sets of ≤5 causal variants at 5 rheumatoid arthritis and 10 type 1 diabetes loci. We identified potentially causal missense variants at *DNASE1L3*, *PTPN22*, *SH2B3*, and *TYK2*, and noncoding variants at *MEG3*, *CD28–CTLA4*, and *IL2RA*. We also identified potential candidate causal variants at *SIRPG* and *TNFAIP3*. Using functional assays, we confirmed allele-specific protein binding and differential enhancer activity for three variants: the *CD28–CTLA4* rs117701653 SNP, *MEG3* rs34552516 indel, and *TNFAIP3* rs35926684 indel.

Rheumatoid arthritis is an autoimmune disease with citrullinated peptide reactivity where chronic inflammation leads to joint destruction[5]. Type 1 diabetes (T1D) arises through autoimmune reactivity to proinsulin[6] and glutamic acid decarboxylase[7], leading to destruction of pancreatic β cells and loss of insulin production. Genome-wide association studies have identified 101 rheumatoid arthritis loci[3,8] and 53 T1D loci[4]; these alleles implicate CD4+ T-cell function in autoimmunity[9–11]. However, causal variants for most loci have yet to be defined. Pinpointing them will enable mechanistic investigation to identify the specific genes, regulatory structures, and genetic mechanisms central to autoimmunity.

Bayesian fine-mapping has been successfully applied to prioritize associated variants in complex diseases[1,12–14]. We fine-mapped 76 autosomal non-major-histocompatibility-complex loci in rheumatoid arthritis (11,475 cases, 15,870 controls)[3] and T1D (9,334 cases, 11,111 controls) (Supplementary Table 1)[4], covering 46 and 49 loci with known rheumatoid arthritis and T1D associations, respectively (Supplementary Table 2). To enable accurate comprehensive imputation, we used individuals genotyped on ImmunoChip, with dense SNP coverage in selected autoimmune disease loci. Our sample size is smaller than the largest of previously published association analyses[4,8]. However, Okada et al.[8] used imputed genotypes but did not define credible sets, and while Onengut-Gumuscu et al.[4] determined credible sets, they did not use imputation so their study included fewer than half of the variants assessed here. We fine-mapped rheumatoid arthritis and T1D together since potential causal variants for both diseases overlap functional elements in CD4+ T cells[11].

Since fine-mapping methods are highly sensitive to missing data, we benchmarked different imputation strategies. After sequencing 799 1-kilobase regulatory (H3K4me3) regions in 568 individuals within these loci, we observed that the 1000 Genomes cosmopolitan reference panel yielded the best results (Fig. 1), while indels and multi-allelic variants remain challenging to impute (Supplementary Note, Supplementary Tables 3–7, and Supplementary Figs. 1–4).

After imputation, we calculated association statistics for 66,923 variants for rheumatoid arthritis and 66,942 variants for T1D (minor allele frequency (MAF) > 1%, imputation quality score (INFO) > 0.3; Hardy–Weinberg $P > 10^{-5}$) at 76 loci. In rheumatoid

[1]Center for Data Sciences, Brigham and Women's Hospital, Harvard Medical School, Boston, MA, USA. [2]Division of Genetics, Brigham and Women's Hospital, Harvard Medical School, Boston, MA, USA. [3]Program in Medical and Population Genetics, Broad Institute of Harvard and MIT, Cambridge, MA, USA. [4]Division of Rheumatology, Immunology, and Allergy, Brigham and Women's Hospital, Harvard Medical School, Boston, MA, USA. [5]Department of Genetics, University of Groningen, University Medical Center Groningen, Groningen, The Netherlands. [6]Department of Public Health Sciences, University of Virginia, Charlottesville, VA, USA. [7]Center for Public Health Genomics, University of Virginia, Charlottesville, VA, USA. [8]The Feinstein Institute for Medical Research, Northwell Health, Manhasset, NY, USA. [9]Arthritis Research UK Centre for Genetics and Genomics, Centre for Musculoskeletal Research, Manchester Academic Health Science Centre, The University of Manchester, Manchester, UK. [10]NIHR Manchester Biomedical Research Centre, Manchester University NHS Foundation Trust, Manchester, UK. [11]Instituto de Parasitología y Biomedicina López-Neyra, Consejo Superior de Investigaciones Científicas, Granada, Spain. [12]Department of Rheumatology, Leiden University Medical Centre, Leiden, The Netherlands. [13]Rheumatology Unit, Department of Medicine, Karolinska Institutet and Karolinska University Hospital, Stockholm, Sweden. [14]Department of Public Health and Clinical Medicine, Division of Rheumatology, Umeå University, Umeå, Sweden. [15]Department of Human Genetics, University of Utah, Salt Lake City, UT, USA. [16]Department of Biomedical Informatics, University of Utah, Salt Lake City, UT, USA. [17]JDRF/Wellcome Diabetes and Inflammation Laboratory, Wellcome Centre for Human Genetics, Nuffield Department of Medicine, University of Oxford, Oxford, UK. [18]Division of Immunology, Boston Children's Hospital, Boston, MA, USA. [19]Department of Biomedical Informatics, Harvard Medical School, Boston, MA, USA. [20]These authors contributed equally: Harm-Jan Westra, Marta Martínez-Bonet. *e-mail: soumya@broadinstitute.org
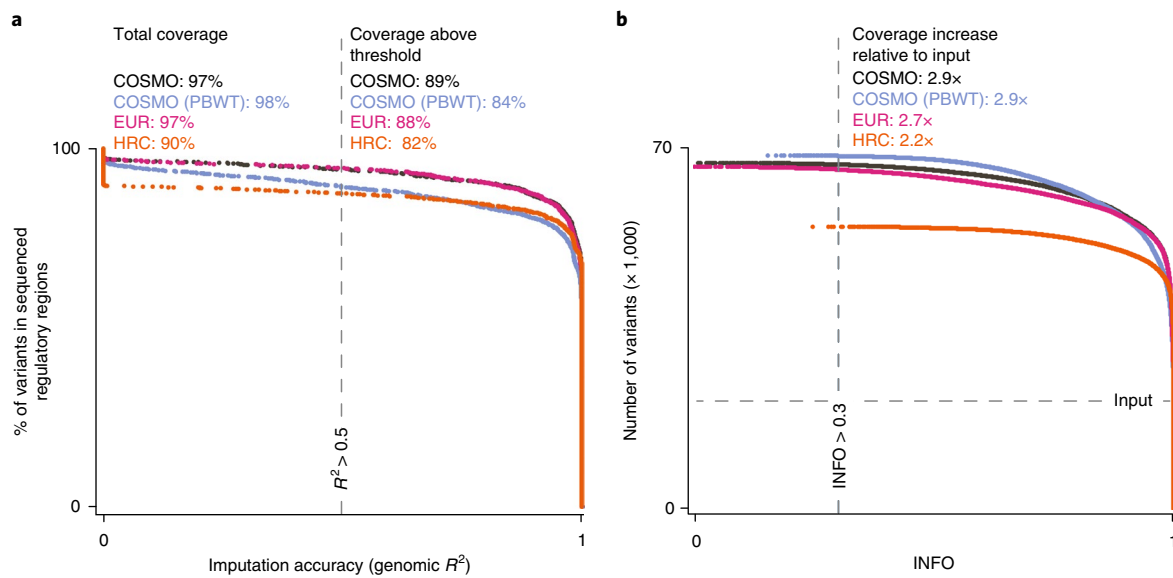
Fig. 1 | Imputation accuracy and quality of datasets. Datasets were imputed with different reference panels: the European subpopulation of 1000 Genomes (EUR), full 1000 Genomes (COSMO), full 1000 Genomes imputed with PBWT (COSMO(PBWT)), and HRC. **a**, We sequenced 799 1-kilobase regions in 568 individuals with ImmunoChip genotypes and called 1,854 common (MAF > 1%) variants. We calculated the imputation accuracy (genomic R^2) by correlating imputed genotypes using each reference panel with genotypes called from the sequencing experiment. **b**, INFO scores for each reference panel in the rheumatoid arthritis dataset.

arthritis and T1D, respectively, we identified 20 and 34 significant loci ($P < 7.5 \times 10^{-7}$), mostly consistent with previous studies (Supplementary Note and Supplementary Table 8). Using approximate Bayesian fine-mapping, we assigned posterior probabilities and defined a 95% credible set for each locus[1,2].

Seven loci were significantly associated with both diseases (*PTPN22*, *AFF3*, *CD28–CTLA4*, *BACH2*, *RASGRP1*, *PTPN2*, and *TYK2*). Rheumatoid arthritis and T1D variant effect sizes were positively correlated in 64% of the tested loci (Methods, Supplementary Table 9, and Supplementary Fig. 5), suggesting shared signals. To prioritize possible shared causal variants, we analyzed a combined dataset (20,787 rheumatoid arthritis or T1D cases, and 18,616 controls; Methods) and observed significant associations at 28 loci. Most (62%) associated variants in these loci were in linkage disequilibrium with the strongest associated variant in either rheumatoid arthritis or T1D (coefficient of determination (R^2) > 0.8; Supplementary Table 10). The combined analysis indicated a potential shared signal at the *PRKCQ* locus (Supplementary Note) that was not significant in rheumatoid arthritis or T1D alone. We did not identify additional significant loci. We did not observe residual population stratification by combining both datasets (Supplementary Note, Supplementary Table 11, and Supplementary Fig. 6). Multinomial Bayesian fine-mapping accounting for opposing effects[15] did not identify additional loci (Supplementary Note and Supplementary Table 12). Because six out of seven shared loci had smaller credible sets in the combined analysis than for the individual disease analyses (Supplementary Note), we decided to use the combined analysis for those six loci.

We narrowed down the list of probable causal variants to ≤5 in 5 out of 20 significant rheumatoid arthritis loci and 10 out of 34 significant T1D loci. We subsequently limited the analysis to 9 (rheumatoid arthritis), 14 (T1D), and 11 (combined) loci with ≤10 variants in the credible sets (Fig. 2a,b and Supplementary Table 13). Credible sets for these loci were not markedly altered when considering variants unique to the Haplotype Reference Consortium (HRC) reference panel (Supplementary Fig. 7 and Supplementary Table 14). To systematically investigate candidate causal variants for both diseases, we selected those with a posterior probability of >0.2

(Table 1). We considered variants to be potentially causal if they: (1) were a missense coding variant; or (2) were in a region with evidence of enhancer activity, and demonstrated allele-specific binding in electrophoretic mobility shift assays (EMSAs) and allele-specific enhancer function in luciferase assays (Supplementary Table 15). Approximate Bayesian fine-mapping assumes a single causal variant per locus, although multiple independent causal variants may be present. Therefore, we applied conditional analysis, exhaustive testing of all variant pairs, FINEMAP[16] (which assumes multiple variants), and haplotype analysis for regions where there was evidence of a secondary effect ($P < 1.9 \times 10^{-5}$).

We identified 42 variants at 20 loci with a posterior probability of >0.2 (Table 1), including 5 missense variants (*PTPN22*, *DNASE1L3*, *SH2B3*, *TYK2*, and *SIRPG*), 3 indels (*ANKRD55*, *TNFAIP3*, and *MEG3*), and 34 noncoding SNP variants (*PTPN22*, *IL10*, *IFIH1*, *CD28–CTLA4*, *ANKRD55*, *BACH2*, *CCL21*, *IL2RA*, *INS*, *SH2B3*, Chr13, *MEG3*, *CTSH*, *TYK2*, *SIRPG*, *UBASH3A*, and *C1QTNF6*). We observed a 16-fold posterior probability enrichment for missense variants. Potentially causal missense variants at *PTPN22*, *SH2B3*, and *TYK2* are well described in the literature[4,17–19] (Supplementary Note and Supplementary Figs. 8–10). We also noted potentially causal missense variants in *DNASE1L3* and *SIRPG*.

DNASE1L3 encodes a nuclease that cleaves double-stranded DNA during apoptosis[20]. The 3p14 *DNASE1L3* locus confers rheumatoid arthritis susceptibility without evidence of a T1D effect ($P > 0.02$; Supplementary Fig. 11). The reported[3] lead SNP rs35677470, encoding an p.Arg206Cys change in DNASE1L3, has a high posterior probability ($P = 1.8 \times 10^{-8}$; posterior probability = 0.82; Supplementary Table 13) and is in linkage disequilibrium with another reported[8] lead variant, rs73081554 ($R^2 = 0.79$). Conditioning on p.Arg206Cys obviates any evidence of independent risk variants ($P > 5 \times 10^{-4}$; Supplementary Table 16). p.Arg206Cys has been implicated in systemic sclerosis[21]; other loss-of-function DNASE1L3 mutations have been reported in familial forms of systemic lupus erythematosus[22]. p.Arg206Cys is a loss-of-function variant that abolishes the protein's nuclease activity[23].

Within 20p13, we identified a p.Val263Ala signal-regulatory protein gamma (SIRPG) missense variant with modest posterior
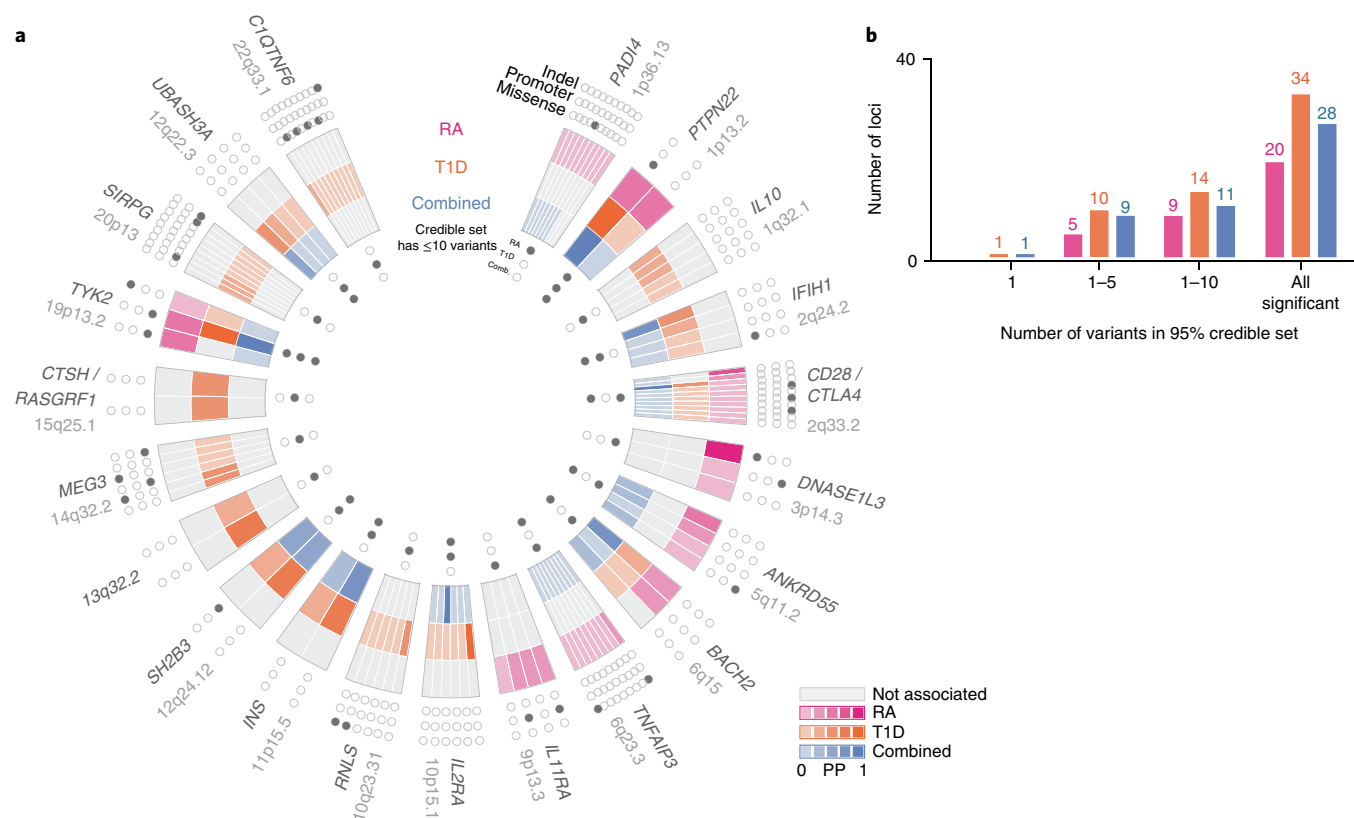
Fig. 2 | Variants in the 95% credible sets of significant loci determined by the Bayesian factor. a, The inner ring of dots indicates whether the locus has ≤10 variants in the credible set and a significant association signal (filled circles). Comb., combined; RA, rheumatoid arthritis. The middle ring shows variants in each credible set. Highlighted segments indicate loci with a candidate causal variant. The color intensity indicates the posterior probability (PP), gray representing a lack of significance. The outer ring shows indel, promoter, and missense coding annotation for each variant in the credible set. **b**, Number of variants in the 95% credible sets within significant loci. We narrowed down the list of probable causal variants to ≤5 in 5 out of 20 significant RA loci, and 10 out of 34 significant T1D loci.

probability (rs6043409; $P = 3.9 \times 10^{-10}$; posterior probability = 0.24) for T1D (Supplementary Fig. 12 and Supplementary Table 13). Conditional analysis using rs6043409 obviated any association signal in the locus ($P > 2 \times 10^{-3}$). p.Val263Ala is in the D3 domain[24]. While D3 has unknown function, homologous D1 and D2 immunoglobulin-like domains mediate interaction with CD47 ligands and SIRPG dimerization[25–27]. We observed linkage disequilibrium ($R^2 > 0.8$) with protein quantitative trait loci (QTL) and expression QTL (eQTL) SNPs (Supplementary Table 17), suggesting that p.Val263Ala might cause a SIRPG conformational change that alters stability, structure, or function. Since p.Val263Ala has unknown function, the two noncoding variants in the *SIRPG* credible set with comparable posterior probabilities and regulatory effects may potentially be causal. However, given the enrichment of missense variants in our data and elsewhere[28,29], we consider p.Val263Ala as the strongest candidate causal variant at this locus.

We identified noncoding alleles with allele-specific function at *CTLA4–CD28*, *TNFAIP3*, and *MEG3* in regions with evidence of CD4+ T-cell enhancer function (Table 1). We identified the rs61839660 variant at *IL2RA* with a high posterior probability (0.85), which was recently demonstrated to have allele-specific regulatory and cellular functions confirmed by CRISPR assays[30]. Detailed analyses of all other loci with ≤10 variants in the 95% credible set are presented in the Supplementary Note and Supplementary Figs. 13–24.

CD28 and *CTLA4* are central to the regulation and differentiation of T cells[20]. The 2q33.2 *CD28–CTLA4* locus is shared by rheumatoid arthritis and T1D[31]. In the combined analysis, a single

variant had a high posterior probability (rs3087243; $P = 1.4 \times 10^{-16}$; posterior probability = 0.91) near *CTLA4*, which also has the largest posterior probability in T1D ($P = 1.6 \times 10^{-15}$; posterior probability = 0.48; Fig. 3a, Supplementary Fig. 25a, and Supplementary Table 13), but not in rheumatoid arthritis ($P = 1.6 \times 10^{-8}$; posterior probability = 0.02). In contrast, rs117701653 near *CD28* ($R^2 = 0.03$ with rs3087243) carried the highest posterior probability in rheumatoid arthritis ($P = 3.5 \times 10^{-10}$; posterior probability = 0.67). In conditional analysis on rs3087243, rs117701653 demonstrated an independent effect ($P = 4.0 \times 10^{-8}$; Fig. 3a and Supplementary Table 16). The FINEMAP[16] program identified the rs117701653 + rs3087243 pair as having the highest posterior probability (0.05; Supplementary Table 18), consistent with an analysis where we tested all SNP pairs exhaustively in rheumatoid arthritis (Fig. 3b and Supplementary Fig. 25b). Haplotype analysis demonstrated independent protective effects of rs3087243-A and rs117701653-C alleles in rheumatoid arthritis and T1D (Fig. 3c), suggesting that rs117701653 might similarly influence T1D risk ($P = 0.03$ in the conditional haplotype analysis). A previous association study identified rs1980422 as the variant with the strongest association in the *CD28* region[8] ($R^2 = 0.02$ with rs117701653 and $R^2 = 0.04$ with rs3087243). Haplotype analysis indicated that rs1980422 imperfectly tags high-frequency haplotypes defined by rs3087243 and rs117701653 (Supplementary Fig. 25c). Both rs117701653 and rs3087243 overlap H3K4me3 peaks in immune cells and disrupt protein-binding motifs (Supplementary Tables 19–25 and Supplementary Note). Only rs3087243 was in linkage disequilibrium with an eQTL (*CTLA4* in CD4+ and CD8+ cells and testis; $R^2 > 0.8$; Supplementary Table 17).

Table 1 | Overview of potentially causal variants at loci having significant association and 95% credible sets with ≤10 variants

PP > 0.2	Potentially causal	Locus	Marker gene(s)	Variant	Disease association	Alleles	Previously identified as top variant	OR for RA	OR for T1D	PP for RA	PP for T1D	PP combined	Variant type
RA		1p13.2	PTPN22	rs6679677	RA + T1D	C, A		1.60	1.95	0.48			Noncoding
RA + T1D	RA + T1D			rs2476601	RA + T1D	G, A	Ref. [8]	1.60	1.95	0.52	0.92	0.90	p.Arg620Trp
T1D		1q32.1	IL10	rs3024505	T1D	G, A	Ref. [4]	1.02	0.85		0.29		Noncoding
T1D				rs3024495	T1D	C, T		1.02	0.85		0.31		Noncoding
T1D				rs3024493	T1D	C, A		1.02	0.85		0.32		Noncoding
T1D		2q24.2	IFIH1	rs2111485	T1D	G, A	Ref. [4]	0.96	0.85		0.46	0.74	Noncoding
T1D				rs984971	T1D	A, G		0.97	0.85		0.31		Noncoding
RA		2q33.2	CD28 CTLA4	rs55686954	RA	G, A		0.75	0.80	0.27			Noncoding
RA	RA			rs117701653	RA	A, C		0.74	0.79	0.67			Noncoding
T1D				rs3087243	T1D; RA (secondary)	G, A	Refs. [4,8]	0.90	0.85		0.48	0.91	Noncoding
RA	RA	3p14.3	DNASE1L3	rs35677470	RA	G, A		1.21	1.01	0.82			p. Arg206Cys
T1D		5q11.2	ANKRD55	rs10213692	RA + T1D	T, C		0.81	0.90		0.34		Noncoding
				rs11377254	RA + T1D	A, AT		0.79	0.89			0.25	Indel
RA				rs7731626	RA + T1D	G, A	Ref. [8]	0.80	0.90	0.41		0.29	Noncoding
		6q15	BACH2	rs10944479	T1D	G, A		1.12	1.19			0.21	Noncoding
RA				rs72928038	RA + T1D	G, A	Ref. [4]	1.13	1.20	0.37	0.27	0.61	Noncoding
RA				rs6908626	RA + T1D	G, T		1.14	1.21	0.29			Noncoding
RA	RA	6q23.3	TNFAIP3	rs35926684	RA	GA, G		1.16	1.06	0.24			Indel
RA		9p13.3	CCL21	rs10972201	RA	G, A		1.12	0.97	0.34			Noncoding
RA				rs2812378	RA	A, G		1.12	0.98	0.36			Noncoding
RA				rs11574914	RA	G, A	Ref. [8]	1.12	0.97	0.25			Noncoding
T1D	T1D	10p15.1	IL2RA	rs61839660	T1D	G, A		0.93	0.64		0.85		Noncoding
RA				rs706778	T1D	C, T	Ref. [8]	1.09	1.22	0.27		0.89	Noncoding
T1D		10q23.31	RNLS	rs12416116	T1D	C, A	Ref. [4]	1.01	0.85		0.46		Noncoding
T1D		11p15.5	INS–IGF2	rs3842753	T1D	T, G		0.98	2.22		0.73	0.77	Noncoding
T1D				rs689	T1D	A, T	Ref. [4]	0.98	2.21		0.27	0.23	Noncoding
T1D	T1D	12q24.12	SH2B3	rs3184504	T1D	A, G		1.04	0.76		0.33	0.45	p.Arg262Trp
T1D				rs653178	T1D	G, A	Ref. [4]	1.04	0.76		0.66	0.54	Noncoding
T1D		13q32.3	–	rs9517712	T1D	T, C		1.03	0.87		0.34		Noncoding
T1D				rs9585056	T1D	A, G	Ref. [4]	0.96	1.16		0.65		Noncoding
T1D		14q32.2	MEG3	rs56994090	T1D	T, C	Ref. [4]	1.01	0.88		0.44		Noncoding
T1D	T1D			rs34552516	T1D	TC, T		1.00	0.88		0.42		Indel
T1D		15q25.1	CTSH	rs34843303	RA	A, G		0.98	0.78		0.45		Noncoding
RA				rs34593439	RA	G, A	Ref. [4]	0.99	0.77		0.51		Noncoding
RA + T1D	RA + T1D	19p13.2	TYK2	rs34536443	RA + T1D	C, G	Refs. [4,8]	0.71	0.64	0.41	1.00	1.00	p. Pro1104Ala
	RA			rs35018800	RA (secondary)	G, A							p.Ala928Val
RA	T1D			rs12720356	Combined (secondary)	A, C	Ref. [4]						p.Ile684Ser
RA				rs45524632	RA	C, A		0.54	0.69	0.53			Noncoding
T1D		20p13	SIRPG	rs6043405	T1D	T, C		1.02	1.15		0.26		Noncoding
T1D				rs6110697	T1D	T, C		1.02	1.15		0.23		Noncoding
T1D	T1D			rs6043409	T1D	A, G	Ref. [4]	1.02	0.87		0.24		p.Val263Ala
T1D		21q22.3	UBASH3A	rs80054410	T1D	A, G		1.06	1.16		0.41	0.59	Noncoding
T1D				rs11203203	T1D	G, A		1.05	1.16		0.39		Noncoding
T1D		22q12.3	C1QTNF6	rs229533	T1D	A, C	Ref. [4]	0.99	1.15		0.23		Noncoding

We declare variants at these loci as potentially causal when they are coding and have a posterior probability (PP) of >0.2, or when they are noncoding, have a PP of >0.2, and have functional evidence from the EMSA and luciferase assays. Logistic regression odds ratio (OR) values are from a two-sided χ^2 test (combined, $n = 39,403$; T1D, $n = 20,445$; rheumatoid arthritis (RA), $n = 27,345$).
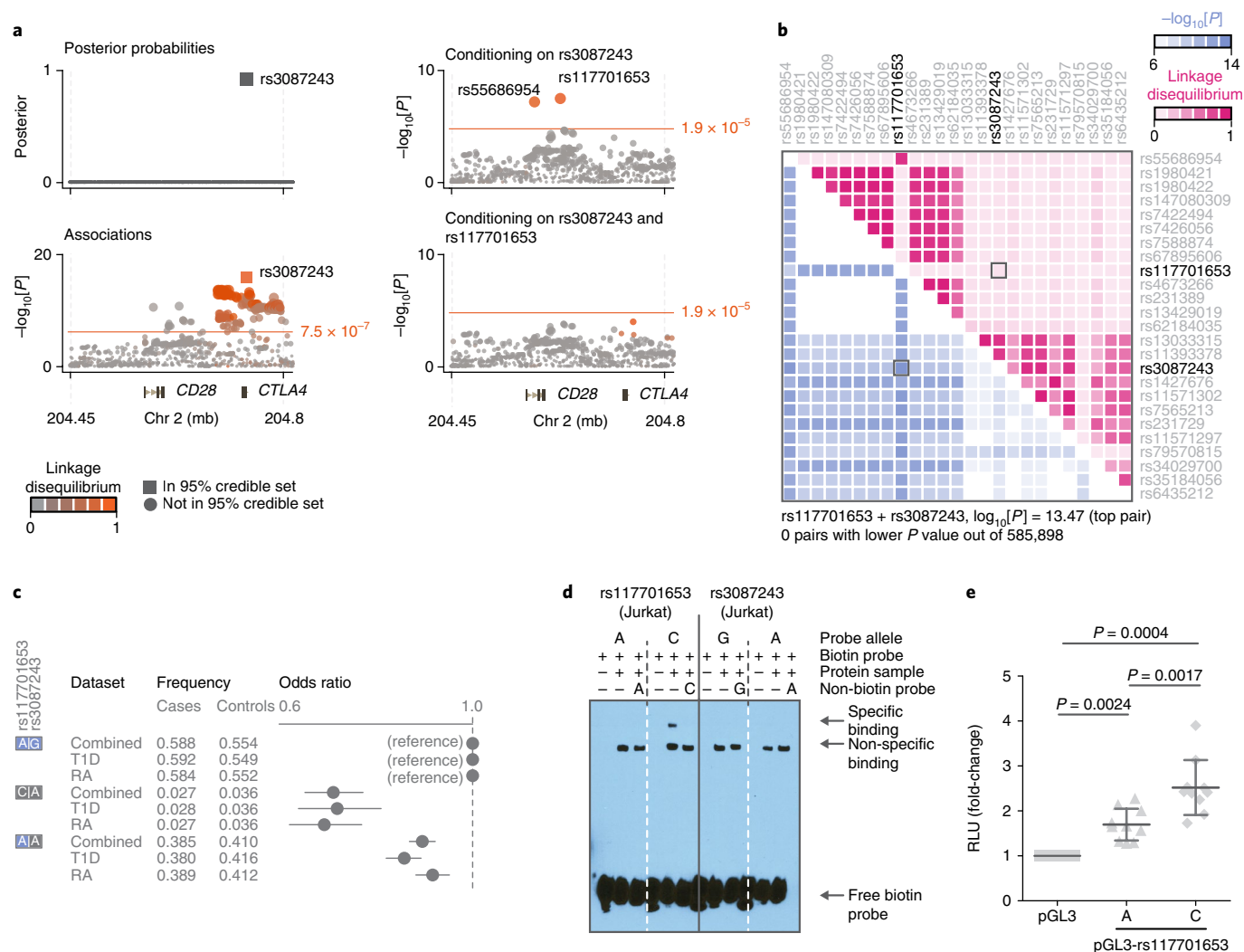
Fig. 3 | Analysis of the *CD28–CTLA4* locus. a, A regional association plot for the combined analysis (20,787 rheumatoid arthritis or T1D cases, and 18,616 unique controls; Methods) shows a single variant (rs3087243) near *CTLA4* in the credible set. Conditioning on rs30872043 identifies rs117701653 as an independent association. Logistic regression $-\log_{10}[P]$ values are from a two-sided χ^2 test ($n = 39,403$). **b**, An exhaustive pairwise analysis for rheumatoid arthritis shows that the rs3087243 + rs117701653 pair has the strongest association. Logistic regression $-\log_{10}[P]$ values are from a two-sided χ^2 test ($n = 27,345$). **c**, Haplotype analysis using rs30872043 and rs117701653, with the AG haplotype as a reference. The C allele of rs117701653 shows the largest decrease in risk for rheumatoid arthritis (RA), and the A allele of rs30872043 shows the largest decrease in risk for T1D. Logistic regression odds ratios (dots) and 95% confidence intervals (bars) are from a two-sided χ^2 test (combined $n = 39,403$; T1D $n = 20,445$; RA $n = 27,345$). **d**, EMSA with Jurkat nuclear extract using probes containing rs117701653 and rs3087243. A representative blot of three independent experiments is shown. **e**, Luciferase assay in Jurkat T cells transfected with pGL3 plasmids containing rs117701653. RLUs are normalized to cells transfected with the empty plasmid (pGL3). Dots represent independent experiments, each of which was performed in duplicate. Means ± s.d. and two-tailed P values of the grouped comparisons (unpaired t-test) are shown.

We observed allele-specific protein binding and enhancer activity for rs117701653, but not rs3087243 (Fig. 3d). The rs117701653-C allele showed higher specific binding than the A allele in Jurkat T-cell nuclear extracts by EMSA (Supplementary Fig. 25d) and conferred higher luciferase expression ($P = 0.0017$; Fig. 3e). The binding is lineage specific: it was absent in THP-1 monocytic cells (Supplementary Fig. 25d). We observed peak overlap in an assay for transposase-accessible chromatin sequencing (ATAC-Seq) for rs117701653 in CD4^{+} T cells (Supplementary Table 25) and a subtle increase in luciferase expression with the C allele after anti-CD3/CD28 cell stimulation ($P = 0.02$; Supplementary Fig. 25e), suggesting that binding may be stimulation dependent. While the rheumatoid arthritis credible set variant rs55686954 ($R^2 = 0.91$ with rs117701653, posterior probability = 0.27) showed allele-specific protein binding, it had no evidence of allele-specific enhancer

function (Supplementary Fig. 25d,e). Promoter-capture Hi-C assays[32] demonstrated genomic contacts between the rs117701653 region and the *CTLA4* promoter and a region downstream of *RAPH1* (Supplementary Fig. 26), suggesting that, despite its proximity to *CD28*, the allele may influence *CTLA4* or *RAPH1* gene regulation.

MEG3 is a noncoding RNA tumor suppressor gene whose transcript binds p53 (ref. [33]). Paternal alleles carry greater risk[34] in this 14q32.2 T1D locus. It shows no association to rheumatoid arthritis ($P > 0.04$). Two variants with >0.2 probabilities in the credible set were the rs34552516 indel ($P = 1.1 \times 10^{-9}$; posterior probability = 0.42) and rs56994090 intronic variant ($P = 1.1 \times 10^{-9}$; posterior probability = 0.44; linkage disequilibrium with rs34552516, $R^2 = 0.99$; Fig. 4a, Supplementary Fig. 27a, and Supplementary Table 12). While we observed no evidence of independent variants conditioning on rs34552516 ($P > 0.04$; Supplementary Table 13),
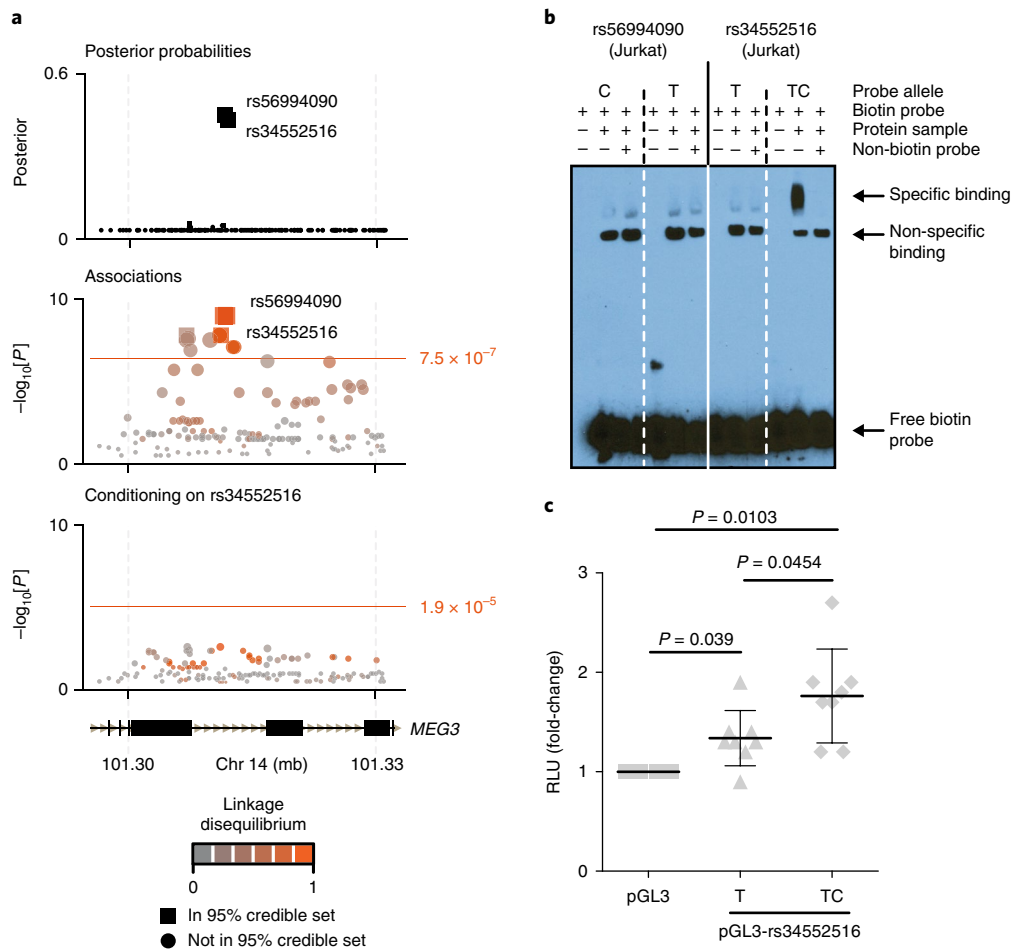
Fig. 4 | Analysis of the *MEG3* locus. a, Regional plot for the *MEG3* locus in T1D (9,334 cases, 11,111 controls). We observe two variants in the credible set (rs56994090 and the rs34552516 indel). We did not observe secondary signals when conditioning on rs56994090. Logistic regression $-\log_{10}[P]$ values are from a two-sided χ^2 test ($n = 20,445$). **b**, EMSA with Jurkat nuclear extract using probes containing rs354552516 and rs56994090. A representative blot of three independent experiments is shown. **c**, Luciferase assay in Jurkat T cells transfected with pGL3 plasmids containing rs34552516. RLUs are normalized to cells transfected with the empty plasmid (pGL3). Dots represent independent experiments, each of which was performed in duplicate. Means ± s.d. and two-tailed *P* values of the grouped comparisons (unpaired *t*-test) are shown.

FINEMAP analysis could not exclude the possibility of a secondary association (Supplementary Table 18 and Supplementary Note). Both *MEG3* variants overlap DNAse-I hypersensitive sites (DHS) and H3K4me3 regions in multiple cell types (Supplementary Tables 20 and 21), but do not overlap ATAC-Seq peaks after stimulation (Supplementary Table 25) and are not in high linkage disequilibrium ($R^2 > 0.8$) with QTL SNPs.

We observed that the rs34552516-TC allele demonstrated specific Jurkat cell nuclear extract binding (Fig. 4b) and increased luciferase activity compared with empty vector ($P = 0.01$) and the T allele ($P < 0.05$; Fig. 5c). We observed no specific binding in THP-1 cells (Supplementary Fig. 27b), indicating cell-type specificity. In contrast, we observed no allele-specific binding for rs56994090 (Fig. 4b). The region harboring rs34552516 in promoter-capture Hi-C data[32] showed contacts to *DIO3* and *RP11-1029J19* promoters (Supplementary Fig. 26), suggesting multiple downstream genes. We favor rs34552516 as potentially causal based on our functional evidence, but acknowledge that these assays are limited and cannot exclude rs56994090 function that may occur in other unexamined cellular contexts.

The 6q23.3 *TNFAIP3* gene encodes A20, which inhibits nuclear factor-κB signaling and prevents apoptosis[20]. It is associated with multiple autoimmune diseases[35–41], including rheumatoid arthritis, but not T1D ($P > 2.3 \times 10^{-4}$). The indel rs35926684 carries the highest

posterior probability ($P = 6.5 \times 10^{-12}$; posterior probability = 0.24; Fig. 5a, Supplementary Table 13, and Supplementary Fig. 28a) of 9 variants in the credible set and is in linkage disequilibrium with the previously identified SNPs rs17264332 ($R^2 = 0.86$)[8] and rs6920220 ($R^2 = 0.88$)[3]. Conditional analysis identified independent association at rs58721818 ($P = 3.6 \times 10^{-5}$; $R^2 = 0.05$ with rs35926684; Fig. 5a and Supplementary Table 16). A previous study[3] identified secondary signals at rs5029937 (linked to rs58721818; $R^2 = 0.84$) and rs13207033. Exhaustive pairwise analysis demonstrated comparable association for the rs35926684 + rs58721818 pair ($-\log_{10}[P] = 13.95$) and the most strongly associated rs6920220 + rs58721818 pair ($-\log_{10}[P] = 14.21$; Fig. 5b and Supplementary Fig. 28b). Haplotypes with the rs35926684-G allele increased rheumatoid arthritis risk, even in absence of the highly linked rs6920220-A risk allele (that is, GGGC versus GAGC; Fig. 5c), although this effect was not significant in conditional haplotype analysis ($P = 0.14$). Consistent with our exhaustive pairwise search, FINEMAP identified the rs35926684 + rs58721818 combination as having the thirteenth highest posterior probability (Supplementary Table 18).

The rs35926684 indel alters binding motifs, overlaps enhancer marks and Encyclopedia of DNA Elements transcription factor binding site (TFBS) chromatin immunoprecipitation sequencing peaks in immune cell types (Supplementary Note and Supplementary Tables 20, 21, and 23–25), and is in linkage disequilibrium ($R^2 > 0.8$)
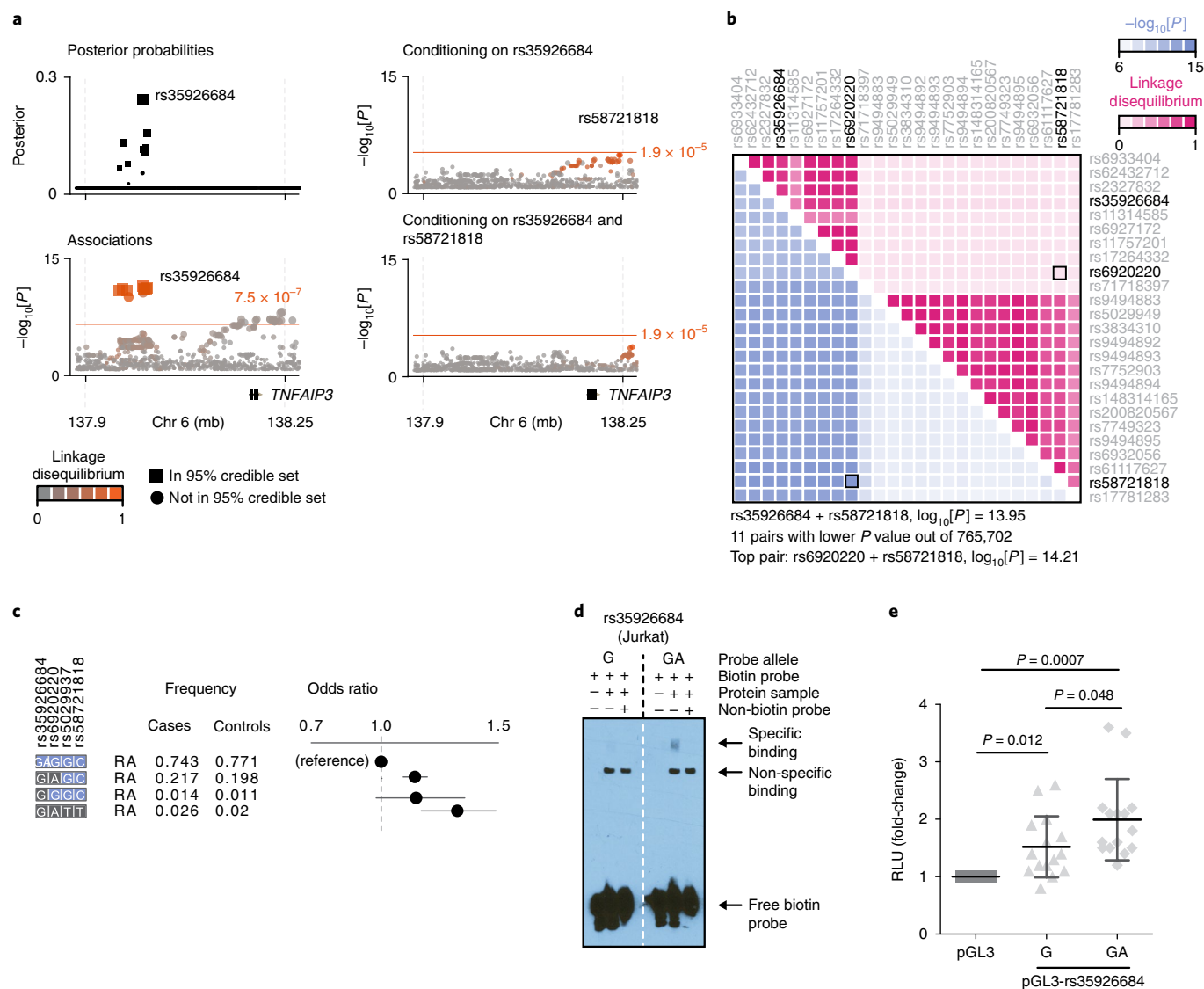
Fig. 5 | Analysis of the *TNFAIP3* locus. a, Regional plot for the *TNFAIP3* locus in rheumatoid arthritis (11,475 cases, 15,870 controls). The variant with the strongest posterior probability in this locus is rs35926684, a G/GA indel. Conditional on rs35926684, we observe a significant secondary association with rs58721818. Logistic regression $-\log_{10}[P]$ values are from a two-sided χ^2 test ($n = 27,345$). **b**, Exhaustive pairwise association analysis in rheumatoid arthritis indicates that there are 11 pairs with a lower *P* value than rs35926684 + rs58721818, although the top-associated pair (rs69220220 + rs58721818) has an equivalent *P* value $-\log_{10}[P] = 13.95$ versus 14.21. Logistic regression $-\log_{10}[P]$ values are from a two-sided χ^2 test ($n = 27,345$). **c**, Haplotype analysis with rs35926684 + rs58721818 and previously reported variants rs6920220 and rs5029937 shows that rs35926684 and the previously reported top variant rs6920220 are often located on the same haplotype (GAGC), although a rare haplotype exists with only the alternative allele of rs35926684, which causes a similar increase in risk, but with a larger confidence interval. Logistic regression odds ratios (dots) and 95% confidence intervals (bars) are from a two-sided χ^2 test ($n = 27,345$). RA, rheumatoid arthritis **d**, EMSA with Jurkat nuclear extract using probes containing the G or GA allele of rs35926684. A representative blot of three independent experiments is shown. **e**, Luciferase assay in Jurkat T cells transfected with pGL3 plasmids containing rs35926684. RLUs are normalized to cells transfected with the empty plasmid (pGL3). Dots represent independent experiments, each of which was performed in duplicate. Means ± s.d. and two-tailed *P* values of comparisons (unpaired *t*-test) are shown.

with a methylation QTL in neutrophils (Supplementary Table 17). EMSA identified stronger specific binding of Jurkat-cell nuclear extract for the rs35926684-GA allele than the G allele (Fig. 5d and Supplementary Fig. 28c). Luciferase assays demonstrated increased enhancer activity with the GA allele compared with the empty vector ($P = 7 \times 10^{-4}$) and G allele ($P = 0.053$; Fig. 5e). We observed no specific binding in THP-1 cells, indicating cell-type specificity (Supplementary Fig. 28c). We observed no allele-specific binding for rs6920220 (Supplementary Fig. 28c) or the other four alleles in partial linkage disequilibrium with rs35926684 (posterior probability > 0.1), except for rs62432712. We did not observe allele-specific

enhancer activity for rs62432712 (Supplementary Fig. 28d). Hence, for this locus, we favor rs35926684 as the potentially causal variant since it has the best evidence of allele-specific activity. Nevertheless, the presence of multiple alleles in linkage disequilibrium ($R^2 > 0.86$) provides ambiguity at this locus. Interestingly, in promoter-capture Hi-C data, the rs35926684 region contacts the *TNFAIP3* promoter[42] and the *IL22RA* and *IFNGR1* promoters (Supplementary Fig. 26)[32], suggesting that multiple genes may be influenced by this rheumatoid arthritis risk allele.

Our study illustrates some challenges of fine-mapping. First, only a few loci had ≤10 plausible causal variants, and in even fewer was

it possible to identify promising candidates. Nonetheless, identifying plausible candidates in even a few instances is valuable. Second, we identified multiple potentially causal variants that were indels. Indels are the most likely to be missed or poorly imputed by current imputation reference panels (Supplementary Note), although coverage could improve with more complete reference panels based on high-depth whole-genome sequencing data. Third, since most loci have many plausible variants with low posterior probabilities, strategies to accurately predict causal variation from functional annotations are critical. This will require more precise noncoding maps that define regulatory elements central to the functions of pathogenic cell types.

We used a posterior probability of >0.2 to prioritize variants for functional follow-up, which allowed us to include variants that might have been excluded by fluctuations in calculated probabilities caused by quality control, genotyping error, imputation quality, and parameter choices. This threshold is relatively stringent (only 42 variants passed it in our entire study), and variants with a posterior probability of <0.2 may also be worthy of further investigation. We focused on loci with ≤10 variants in the 95% credible set; 12 loci had >10 variants in the 95% credible set and at least 1 variant with a posterior probability of >0.2 (Supplementary Table 26). In the *RASGRP1* and *PRKQC* credible sets, we observed a single variant with tenfold higher posterior probability than the remaining variants, but we did not investigate these loci in detail since they had weaker association and their credible set size suggests extensive linkage disequilibrium, making determination of the functional impact more difficult.

We used Jurkat T-cell lines for EMSA and luciferase assays since T cells are critical to the genetic etiology of rheumatoid arthritis and T1D. We acknowledge that, in vivo, many contexts may be relevant, some of which may not be captured by these assays. Consequently, many of the remaining variants with a posterior probability of >0.2 are plausible candidates that cannot be ruled out. Furthermore, our study is limited in identifying causal molecular mechanisms and genes. First, variants may be linked to multiple genes. For example, the region harboring the rs117701653 variant shows chromatin contacts with the *CTLA4* promoter and the *RAPH1* gene. Second, only a limited number of prioritized variants were in linkage disequilibrium with different molecular QTLs. As such, the specific gene(s) accounting for disease susceptibility remain(s) to be determined. Despite these limitations, we believe that the combination of statistical evidence with functional follow-up is a powerful way to prioritize potentially causal variants. Defining cellular models that best represent the pathogenic cellular contexts is an essential component for this functional follow-up.

URLs. Bios eQTL browser, http://genenetwork.nl/biosqtl-browser/; Roadmap Epigenomics datasets, http://www.road-mapepigenomics.org/; ChromHMM enhancers and promoters, http://egg2.wustl.edu/roadmap/web_portal/; 1000 Genomes reference panel, http://bochet.gcc.biostat.washington.edu/beagle/1000_Genomes_phase3_v5a/; Haplotype Reference Consortium panel, http://www.haplotype-reference-consortium.org/.

Online content

Any methods, additional references, Nature Research reporting summaries, source data, statements of data availability and associated accession codes are available at https://doi.org/10.1038/s41588-018-0216-7.

References

1. Maller, J. B. et al. Bayesian refinement of association signals for 14 loci in 3 common diseases. *Nat. Genet.* **44**, 1294–1301 (2012).
2. Wakefield, J. A Bayesian measure of the probability of false discovery in genetic epidemiology studies. *Am. J. Hum. Genet.* **81**, 208–227 (2007).
3. Eyre, S. et al. High-density genetic mapping identifies new susceptibility loci for rheumatoid arthritis. *Nat. Genet.* **44**, 1336–1340 (2012).
4. Onengut-Gumuscu, S. et al. Fine mapping of type 1 diabetes susceptibility loci and evidence for colocalization of causal variants with lymphoid gene enhancers. *Nat. Genet.* **47**, 381–386 (2015).
5. Klareskog, L., Catrina, A. I. & Paget, S. Rheumatoid arthritis. *Lancet* **373**, 659–672 (2009).
6. Palmer, J. P. et al. Insulin antibodies in insulin-dependent diabetics before insulin treatment. *Science* **222**, 1337–1339 (1983).
7. Baekkeskov, S. et al. Identification of the 64K autoantigen in insulin-dependent diabetes as the GABA-synthesizing enzyme glutamic acid decarboxylase. *Nature* **347**, 151–156 (1990).
8. Okada, Y. et al. Genetics of rheumatoid arthritis contributes to biology and drug discovery. *Nature* **506**, 376–381 (2014).
9. Hu, X. et al. Integrating autoimmune risk loci with gene-expression data identifies specific pathogenic immune cell subsets. *Am. J. Hum. Genet.* **89**, 496–506 (2011).
10. Finucane, H. K. et al. Heritability enrichment of specifically expressed genes identifies disease-relevant tissues and cell types. *Nat. Genet.* **50**, 621–629 (2018).
11. Trynka, G. et al. Chromatin marks identify critical cell types for fine mapping complex trait variants. *Nat. Genet.* **45**, 124–130 (2013).
12. Huang, H. et al. Fine-mapping inflammatory bowel disease loci to single-variant resolution. *Nature* **547**, 173–178 (2017).
13. Gaulton, K. J. et al. Genetic fine mapping and genomic annotation defines causal mechanisms at type 2 diabetes susceptibility loci. *Nat. Genet.* **47**, 1415–1425 (2015).
14. Farh, K. K. et al. Genetic and epigenetic fine mapping of causal autoimmune disease variants. *Nature* **518**, 337–343 (2015).
15. Jostins, L. & McVean, G. Trinculo: Bayesian and frequentist multinomial logistic regression for genome-wide association studies of multi-category phenotypes. *Bioinformatics* **32**, 1898–1900 (2016).
16. Benner, C. et al. FINEMAP: efficient variable selection using summary data from genome-wide association studies. *Bioinformatics* **32**, 1493–1501 (2016).
17. Begovich, A. B. et al. A missense single-nucleotide polymorphism in a gene encoding a protein tyrosine phosphatase (*PTPN22*) is associated with rheumatoid arthritis. *Am. J. Hum. Genet.* **75**, 330–337 (2004).
18. Bottini, N. et al. A functional variant of lymphoid tyrosine phosphatase is associated with type I diabetes. *Nat. Genet.* **36**, 337–338 (2004).
19. Diogo, D. et al. TYK2 protein-coding variants protect against rheumatoid arthritis and autoimmunity, with no evidence of major pleiotropic effects on non-autoimmune complex traits. *PLoS One* **10**, e0122271 (2015).
20. Sisirak, V. et al. Digestion of chromatin in apoptotic cell microparticles prevents autoimmunity. *Cell* **166**, 88–101 (2016).
21. Zochling, J. et al. An ImmunoChip-based interrogation of scleroderma susceptibility variants identifies a novel association at *DNASE1L3*. *Arthritis Res. Ther.* **16**, 438 (2014).
22. Al-Mayouf, S. M. et al. Loss-of-function variant in *DNASE1L3* causes a familial form of systemic lupus erythematosus. *Nat. Genet.* **43**, 1186–1188 (2011).
23. Ueki, M. et al. Caucasian-specific allele in non-synonymous single nucleotide polymorphisms of the gene encoding deoxyribonuclease I-like 3, potentially relevant to autoimmunity, produces an inactive enzyme. *Clin. Chim. Acta* **407**, 20–24 (2009).
24. Nettleship, J. E. et al. Crystal structure of signal regulatory protein gamma (SIRPγ) in complex with an antibody Fab fragment. *BMC Struct. Biol.* **13**, 13 (2013).
25. Brooke, G., Holbrook, J. D., Brown, M. H. & Barclay, A. N. Human lymphocytes interact directly with CD47 through a novel member of the signal regulatory protein (SIRP) family. *J. Immunol.* **173**, 2562–2570 (2004).
26. Piccio, L. et al. Adhesion of human T cells to antigen-presenting cells through SIRPbeta2–CD47 interaction costimulates T-cell proliferation. *Blood* **105**, 2421–2427 (2005).
27. Liu, Y. et al. Functional elements on SIRPalpha IgV domain mediate cell surface binding to CD47. *J. Mol. Biol.* **365**, 680–693 (2007).
28. Gusev, A. et al. Partitioning heritability of regulatory and cell-type-specific variants across 11 common diseases. *Am. J. Hum. Genet.* **95**, 535–552 (2014).
29. Sveinbjornsson, G. et al. Weighting sequence variants based on their annotation increases power of whole-genome association studies. *Nat. Genet.* **48**, 314–317 (2016).
30. Simeonov, D. R. et al. Discovery of stimulation-responsive immune enhancers with CRISPR activation. *Nature* **549**, 111–115 (2017).
31. Fortune, M. D. et al. Statistical colocalization of genetic risk variants for related autoimmune diseases in the context of common controls. *Nat. Genet.* **47**, 839–846 (2015).
32. Javierre, B. M. et al. Lineage-specific genome architecture links enhancers and non-coding disease variants to target gene promoters. *Cell* **167**, 1369–1384. e19 (2016).

33. Zhou, Y. et al. Activation of p53 by MEG3 non-coding RNA. *J. Biol. Chem.* **282**, 24731–24742 (2007).

34. Wallace, C. et al. The imprinted *DLK1–MEG3* gene region on chromosome 14q32.2 alters susceptibility to type 1 diabetes. *Nat. Genet.* **42**, 68–71 (2010).

35. Tsoi, L. C. et al. Identification of 15 new psoriasis susceptibility loci highlights the role of innate immunity. *Nat. Genet.* **44**, 1341–1348 (2012).

36. Jostins, L. et al. Host–microbe interactions have shaped the genetic architecture of inflammatory bowel disease. *Nature* **491**, 119–124 (2012).

37. Beecham, A. H. et al. Analysis of immune-related loci identifies 48 new susceptibility variants for multiple sclerosis. *Nat. Genet.* **45**, 1353–1360 (2013).

38. Lessard, C. J. et al. Variants at multiple loci implicated in both innate and adaptive immune responses are associated with Sjögren's syndrome. *Nat. Genet.* **45**, 1284–1292 (2013).

39. Cordell, H. J. et al. International genome-wide meta-analysis identifies new primary biliary cirrhosis risk loci and targetable pathogenic pathways. *Nat. Commun.* **6**, 8019 (2015).

40. Bentham, J. et al. Genetic association analyses implicate aberrant regulation of innate and adaptive immunity genes in the pathogenesis of systemic lupus erythematosus. *Nat. Genet.* **47**, 1457–1464 (2015).

41. Trynka, G. et al. Dense genotyping identifies and localizes multiple common and rare variant association signals in celiac disease. *Nat. Genet.* **43**, 1193–1201 (2011).

42. McGovern, A. et al. Capture Hi-C identifies a novel causal gene, *IL20RA*, in the pan-autoimmune genetic susceptibility region 6q23. *Genome. Biol.* **17**, 212 (2016).

Author contributions

H.-J.W., Y.L. and S.R. performed the analyses. M.M.-B. and P.A.N. performed the functional assays. H.-J.W., M.M.-B., P.A.N. and S.R. designed the study. S.O., A.L., N.T., J.W., J.M., T.H., L.K., S.R.-D., W.-M.C., A.Q., J.A.T., S.E., P.K.G., S.S.R. and S.R. acquired the data. H.-J.W., M.M.-B., Y.L., J.A.T., P.A.N., P.K.G., S.S.R. and S.R. wrote and edited the manuscript.

Competing interests

The authors declare no competing interests.

Additional information

Supplementary information is available for this paper at https://doi.org/10.1038/s41588-018-0216-7.

Reprints and permissions information is available at www.nature.com/reprints.

Correspondence and requests for materials should be addressed to S.R.

Publisher's note: Springer Nature remains neutral with regard to jurisdictional claims in published maps and institutional affiliations.

Methods

Ethics. This study complies with all relevant ethical regulations. The study protocol was approved as an exempt study by Brigham and Women's Hospital. Institutional Review Board approval for the original genotyping studies is described separately[3,4].

Patient collections. We used genotyping data from samples collected on the ImmunoChip platform (Supplementary Table 1)[3,4]. For rheumatoid arthritis, we used data for 11,475 cases and 15,870 controls from 6 different cohorts (from the UK, the Swedish Epidemiological Investigation of Reumatoid Arthritis, the USA, the Netherlands, Umeå (Sweden), and Spain)[3]. For T1D, we used data for 12,241 cases and 14,636 controls from 2 different cohorts[4]: the Type 1 Diabetes Genetics Consortium (T1DGC) family collection, and the UK Genetic Resource Investigating Diabetes (GRID), British 1958 Birth Cohort, and UK Blood Service collection. To include trios from the Type 1 Diabetes Genetics Consortium cohort in the case-control analysis, we generated pseudocontrol pairs for each affected individual using the untransmitted alleles from the parents of that individual. As a consequence, the final numbers of individuals for T1D were 9,334 cases and 11,111 controls (including 1,661 pseudocontrols). Genotype quality control was performed as described in the previously published studies. Additionally, we merged the genotype data for the different cohorts within T1D and rheumatoid arthritis using PLINK[43], and converted genomic coordinates using the University of California, Santa Cruz liftOver tool[44] and the hg18ToHg19 chain file. Variants unable to liftOver were removed. We then replaced the variant identifiers using National Center for Biotechnology Information Database of Single Nucleotide Polymorphisms (dbSNP) build 138[45]. Finally, we removed variants with a MAF of <0.5%.

Imputation. To assess the imputation strategy best suited for fine-mapping, we tested three reference panels: (1) the European subpopulation of 1000 Genomes ($n = 503$); (2) the cosmopolitan panel of 1000 Genomes ($n = 2,504$); and (3) the HRC version 1.1 reference panel ($n = 32,611$). We matched variants to each reference panel, removed variants absent in the reference panel, and aligned the strands of the remaining ImmunoChip genotypes. We extended the disease loci upstream and downstream by 1 Mb. We excluded variants when alleles could not be matched. For C/G and A/T variants, we removed the variant when the minor allele was unequal and the MAF was <45%. For multi-allelic variants, we ensured that the allele encoding was identical to the reference panel variant. This resulted in a different number of input variants for each imputation strategy (Supplementary Table 6). We imputed genotypes into rheumatoid arthritis and T1D separately. We phased and imputed the 1000 Genomes reference panels using Beagle version 4.1 (22Apr16.1cf)[46]. To accommodate computational constraints of Beagle, we split the rheumatoid arthritis and T1D datasets into 30 batches, randomizing cases and controls between batches, while maintaining trio structure in the T1D dataset. Since the HRC version 1.1 reference panel genotype data are not publicly available, we evaluated different imputation servers and settings for the T1D dataset, to determine their effects on imputation output. On the Sanger Institute imputation server (date of access: 11 May 2016), we used prephasing with either EAGLE (version 2.3.4)[47] or SHAPEIT (version 2.r837)[48], followed by imputation with PBWT (version 3.0)[49]. On the Michigan University server (date of access: 5 July 2016), we split the dataset into three batches and used prephasing with EAGLE[47] and imputation by MiniMac[50]. For rheumatoid arthritis, we performed HRC imputation on the Sanger imputation server using EAGLE prephasing followed by PBWT imputation. Finally, we locally performed 1000 Genomes imputation by first phasing with EAGLE, and subsequently imputing using PBWT. We then merged the imputed dosages and probabilities from each batch (if any) for each imputation reference panel and replaced the variant identifiers in the imputed output using National Center for Biotechnology Information dbSNP build 138. We replaced genotypes for variants genotyped on ImmunoChip with the original genotypes. Genotyped variants correlated with genotypes after imputation ($R^2 > 0.99$). Finally, we recalculated the imputation quality scores for each imputed variant in each dataset: we used the INFO score for biallelic variants and Beagle version 4.1 allelic-R^2 for multi-allelic variants.

Targeted sequencing. To test the accuracy of imputation, we sequenced 900 regions of 1,000 base pairs (bp) around H3K4me3 peak centers overlapping loci associated with either disease in 864 individuals: 384 unrelated rheumatoid arthritis and 480 T1D individuals (160 trios), of which 149 and 480 were on ImmunoChip, respectively. We generated 100-bp paired-end reads with the Illumina MiSeq platform. Sequencing was performed at The Feinstein Institute for Medical Research at Northwell Health, and at The Center for Public Health Genomics, at the University of Virginia. We used BWA-mem[51] (version 0.7.12) to align reads to the hg19 reference genome. We tagged and removed duplicate reads using Picard MarkDuplicates. We removed samples where >50% of the samples had <20× coverage at >80% of sequenced bases, and removed 86 samples having <20× coverage at 90% of sequenced bases. We called genotypes using GATK version 3.4, following the recommended guidelines for using HaplotypeCaller[52] in a joint genotype-calling approach. To determine the impact of local alignment on indel calls, we also called variants using the UnifiedGenotyper present in

GATK. We then set genotypes with <10× coverage and genotype quality (QUAL) <30 to missing, and excluded variants with >5% missingness. We correlated called genotypes with ImmunoChip genotypes to identify and remove (when the coefficient of correlation (r) < 0.95) possible sample swaps and mismatched samples, resulting in 568 final samples (439 for T1D and 129 for rheumatoid arthritis). Finally, we selected variants with MAF > 1%, resulting in 1,862 variants within the 76 rheumatoid arthritis- and T1D-associated regions.

Combined dataset. Before the association analysis, we merged the data for the rheumatoid arthritis and T1D dataset, imputed with the cosmopolitan reference panel of 1000 genomes. We identified shared controls between datasets by generating a list of linkage disequilibrium pruned variants from the ImmunoChip genotypes using PLINK[43] (using --indep-pairwise 1000 100 0.2) and then used this list to determine the genetic similarity (unified additive relationship)[53] between each pair of samples across both datasets. We considered sample pairs with a unified additive relationship of >0.2 genetically related, and randomly selected one sample of the pair to be included. We considered the remaining sample pairs unrelated. We finally merged genotypes and imputation probabilities from the selected samples and recalculated the imputation INFO scores for the merged genotypes as described earlier.

Fine-mapping and statistical analysis. We limited our association analysis to variants with an overall MAF of >1%, a Hardy–Weinberg P value of >10^{-5} in controls, and an overall INFO score >0.3. The Hardy–Weinberg P value was calculated using an exact test for biallelic variants and a Pearson's chi-squared test for multi-allelic variants. We then split multi-allelic variants, creating a single variant for each alternative allele. To test each variant for association with disease, we used logistic regression, assuming a log-linear relation between the number of alternative alleles and case-control status. In the rheumatoid arthritis dataset, the null model included the first ten principal components calculated over the genotype covariance matrix, as described previously[3], and five additional covariates indicating the cohort. For T1D, we included 12 regional indicator variables in the null model, as described previously[4], and an additional variable indicating the cohort. For the joint analysis, the null model included all covariates for the T1D and rheumatoid arthritis datasets and an additional covariate indicating the sample originating dataset. We recoded the imputation probabilities to a dosage value ranging between 0 and 2 (that is $P(AB) + 2 \times P(BB)$). Finally, we calculated the P value for the association as the difference in deviance between the null model and alternative model containing the imputation probabilities, which follows a chi-squared distribution with one degree of freedom. We corrected for multiple testing using a study-wide Bonferroni threshold using the maximum number of tests across datasets ($P < 7.5 \times 10^{-5} \sim 0.05/67,156$). To test whether our model was properly adjusting for population stratification when performing the combined analysis, we also evaluated using the first 20 principal components as covariates. We obtained principal components with the PLINK[43] –pca command using the non-imputed and pruned combined ImmunoChip genotypes. By also including a covariate indicating the source dataset of each individual, we accounted for any residual technical differences caused by rheumatoid arthritis and T1D samples being genotyped and imputed independently.

Definition of credible sets. To define potentially causal variants for each locus, we calculated posterior probabilities using the approximate Bayesian factor (ABF)[1,2] under the assumption of a single causal variant per locus. This framework assumes that the association effect sizes follow a distribution of $N(0,V)$ under H_0, with V being the squared standard error. Under H_1, the framework assumes a distribution following $N(0, V + W)$, where W is $(\ln[1.5]/1.96)^2$, reflecting the prior of observing an odds ratio of 1.5. The ABF for an observed effect size β is then calculated as the ratio of $P(\beta|H_0)/P(\beta|H_A)$. Using the sum of the ABF for all variants in the locus, we calculate the posterior probability (PP) for variant i as:

$$PP_i = \frac{ABF_i}{\sum_{k=0}^{n} ABF_k}$$

Following calculation of the posterior probability, we created credible sets by sorting associations descending on the basis of their posterior probability and including associations such that the sum of posterior probability was >0.95.

Detecting secondary associations. To determine the presence of multiple independent effects, we performed conditional analyses using logistic regression. For each locus with a significant association, we included the top-associated variant as a covariate in the null and alternative models and repeated the association analysis for that locus. We considered secondary associations significant when $P < 1.9 \times 10^{-5}$ (Bonferroni correction for maximum number of variants in significant loci: 0.05/2,704). We then performed exhaustive pairwise association analyses to test whether the primary and secondary associations together provided the strongest pairwise association signal given all possible pairs of variants in the locus. We calculated a P value using the difference in deviance between the null and alternative models, following a chi-squared distribution with two degrees of freedom.

Finally, for loci with two or more independent associations, we assessed whether the risk alleles for the associated variants were located on the same haplotypes. We derived haplotypes from the phased imputation output (for example, four haplotypes for two independent variants). We removed all haplotypes with a frequency of <1% and individuals having those haplotypes, and used the haplotype with the highest frequency as a reference. We then used logistic regression to test remaining haplotypes for association, assuming a log-linear relationship between the number of haplotype copies and disease status. To correct for population differences, our null model included covariates as described above.

We also performed fine-mapping using FINEMAP version 1.1[16], which allows multiple independent associations per locus. As input, we used the summary statistics for the individual disease association analyses and genotype correlation matrices as linkage disequilibrium estimates. Finally, we assessed whether opposite effects between rheumatoid arthritis and T1D may cause lower power in the combined analysis by applying Trinculo version 0.96[15]—a method that implements multinomial logistic regression. As covariates for this analysis, we used the 20 principal components and indicator variable described above, to prevent multicollinearity.

Overlap with eQTLs, H3K4me3 peaks, DNAse-I hypersensitive sites, enhancers, and motifs. To provide functional annotation for the identified variants, we assessed overlap with eQTLs, H3K4me3 peaks, DNAse-I hypersensitive sites, promoters, and enhancers. We used eQTLs from an RNA sequencing-based eQTL meta-analysis of 2,116 whole blood samples[54], a study assessing eQTLs in CD4^{+} T cells from 461 individuals[55], a study assessing eQTLs in CD4^{+} and CD8^{+} cells from 313 individuals[56], and tissue-specific eQTLs from the Genotype–Tissue Expression (GTEx) project[57]. We also included molecular QTLs, such as histone QTLs, methylation QTLs, and protein QTLs[56,58]. For each variant in a credible set, we considered a QTL to be overlapping when it was in high linkage disequilibrium ($R^2 > 0.8$) with the top QTL for a given gene, methylation probe, histone mark, or protein. For calculation of linkage disequilibrium, we used the European subpopulation of 1000 Genomes.

For further annotation, we determined the overlap of variants with a posterior probability of >0.2 with H3K4me3 peaks, DNAse-I peaks, and ChromHMM[59] genome segmentations from 12 imputed epigenetic marks from the Roadmap Epigenomics Consortium[60], consisting of 127 consolidated epigenomes from different cell types. Furthermore, we determined whether candidate causal variants affected protein-binding motifs or transcription factor binding sites using HaploReg[61]. Finally, we determined overlap with TFBSs using Encyclopedia of DNA Elements project transcription factor chromatin immunoprecipitation sequencing[62] and determined whether these variants overlapped conserved TFBS motifs by defining a 40-bp region around each variant, and using the Homer[63] software to test all known motifs in vertebrates.

ATAC-Seq time series. We applied ATAC-Seq[64] to measure chromatin accessibility in a time series after stimulation. We used a leukopak (30 ml whole blood) from a healthy anonymous donor to isolate peripheral blood mononuclear cells using Ficoll tubes, which were stored in 500 μl aliquots of 100×10^6 cells in liquid nitrogen. Cells were subsequently thawed and stained with anti-biotin microbeads to magnetically select CD4^{+} Tmem cells. Cells were resuspended and transferred to 24-well plates in 3 ml aliquots of 6×10^6 cells and stimulated using Dynabeads (Human T-Activator CD3/CD28 for T Cell Expansion and Activation; Life Technologies) in a ratio of two cells per bead. Samples of 100,000 cells were taken at 0, 1, 2, 4, 8, 12, 24, and 48 h after stimulation. Nucleosome isolation and ATAC-Seq open chromatin sequencing were performed as described earlier[64]. Sequenced reads were mapped to the hg19 reference genome using BWA-mem. Reads mapping to the mitochondrial genome or to multiple genomic locations, and duplicate reads (labeled by Picard MarkDuplicates (version 1.128)) were removed, and reads were shifted +4 and −5 bp for the reverse and forward strands, respectively. Enrichment for open chromatin was determined by calling peaks using MACS version 2.1.0 (ref. [65]) (default settings).

Cell lines. Jurkat and THP-1 cell lines were obtained from the American Type Culture Collection (TIB-152 and TIB-202). Jurkat cells were grown in complete Roswell Park Memorial Institute (RPMI) (RPMI-1640; Gibco, with 10% decomplemented fetal bovine serum, penicillin and streptomycin) and THP-1 cells in complete RPMI supplemented with 2-mercaptoethanol to a final concentration of 0.05 mM. Both cell lines were grown in a 37 °C incubator with 5% CO_2.

EMSAs. EMSAs were performed using the LightShift Chemiluminiscent EMSA Kit (Thermo Scientific). Single-stranded oligonucleotides corresponding to 30–32 nucleotide fragments of the human genome with the SNP of interest in the middle were purchased from Integrated DNA Technologies (Supplementary Table 27) and biotinylated using the Biotin 3′ End DNA Labeling Kit (Thermo Scientific). Double-stranded oligonucleotides were generated by mixing equal amounts of biotin-labeled (for the probe) or unlabeled (for the competitor) complementary oligonucleotides and incubated for 5 min at 95 °C and then 1 h at room temperature.

Nuclear extract from Jurkat and THP-1 cells was obtained using the NE-PER Nuclear and Cytoplasmic Extraction Reagents (Thermo Scientific). Protein extracts were dialyzed using a dialysis membrane with a molecular weight cut-off of 12–14 kDa (Spectrum Spectra) against 1 l of dialysis buffer (10 mM Tris pH 7.5, 50 mM KCl, 200 mM NaCl, 1 mM dithiothreitol, 1 mM phenylmethane sulfonyl fluoride, and 10% glycerol) for 16 h at 4 °C with slow stirring. Protein inhibitor cocktail (Sigma) was added to a final concentration of 2.5×. The protein concentration was measured using the Pierce BCA Protein Assay Kit (Thermo Scientific).

The standard binding reaction contained 2 μl of 10× Binding Buffer (100 mM Tris pH 7.5, 500 mM KCl and 10 mM dithiothreitol), 2.5% glycerol, 5 mM $MgCl_2$, 0.05% NP40, 50 ng Poly(dI:dC), 20 fmol biotin-labeled probe, and 16 μg nuclear extract in a final volume of 20 μl. For competition experiments, a 200-fold molar excess (4 pmol) of unlabeled probe was added. Variations to these conditions are indicated in the corresponding figure (Supplementary Figures 25D, 27B, and 28C).

Binding reactions were incubated at room temperature for 30 min and loaded onto a 6% polyacrylamide 0.5× TBE Gel. After sample electrophoresis and transfer to a nylon membrane, transferred DNA was crosslinked for 10 min, and the biotinylated probes were detected by chemiluminescence followed by film exposure. Original films are presented in Supplementary Fig. 29.

Luciferase reporter assay. The double-stranded oligonucleotide containing the SNP of interest (obtained as described above) was cloned downstream from the luciferase gene in the luciferase reporter vector pGL3 promoter (Promega). Unlabeled double-stranded oligonucleotides containing the corresponding SNPs were amplified with specific primers containing the BamHI restriction site obtained from Integrated DNA Technologies (Supplementary Table 28). The PCR was carried out in 50 μl reaction volume under the following program: 94 °C for 3 min; 10 cycles at 94 °C for 30 s, 60 °C for 40 s, and 68 °C for 30 s; 15 cycles at 94 °C for 30 s, 60 °C for 40 s, and 68 °C for 30 s; and 72 °C for 10 min (AccuPrime Taq; Invitrogen). Both the PCR products and pGL3 promoter vector were digested with BamHI (New England Biolabs) for 1 h at 37 °C, and linearized vector was then dephosphorylated for 30 min at 37 °C with the Quick Dephosphorylation kit (New England Biolabs). Digestion products were purified with the QIAquick Gel Extraction Kit (Qiagen) from 1.2% agarose gels. Ligation of SNP-containing fragments into the pGL3 promoter plasmid was performed in a ratio of 1:50 (vector:insert) with T4 DNA ligase (New England Biolabs) at 16 °C overnight and transformed into JM109 competent cells (Promega). Plasmids from independent colonies were isolated using a Wizard Plus SV Minipreps DNA purification system and sequenced using RV primer 4 (Promega), selecting those harboring the SNP-construct cloned 'in sense' in the pGL3 promoter vector for further HighPure plasmid isolation (Invitrogen).

At least three independent transfection experiments for each construct were performed, each in duplicate. 2×10^4 Jurkat cells in 0.1 ml of complete RPMI were transfected with 0.8 μg of pGL3-Promoter vector along with 0.2 μg of pRL-TK *Renilla* luciferase vector (Promega) using 1.5 μl of Lipofectamine LTX Reagent and 1 μl of PLUS Reagent (both from Invitrogen) diluted in Opti-MEM (Gibco). After 16 h of transfection, luciferase activity was measured using the Dual-Glo Luciferase Assay System (Promega). Firefly luciferase activity was expressed as relative luciferase units (RLU) after correction for *Renilla* luciferase activity to adjust for transfection efficiency. Data were normalized to those cells transfected with empty pGL3-Promoter vector.

For the rs117701653 variant at the *CD28–CTLA4* locus, we also investigated the luciferase signal under stimulatory conditions. We transfected Jurkat cells as described above, and 18 h after transfection, cells were left untreated or stimulated with αCD3/αCD28 (0.5 μg αCD3 coated to the plate and 5 μg ml^{−1} of soluble α CD28) or phytohemagglutinin (2 μg ml^{−1}). Luciferase activity was measured 6 h after stimulation. Four independent experiments were performed in duplicate. The results of individual assays are presented in Supplementary Table 29.

Statistical analysis of functional studies. Luciferase activity levels were compared by unpaired two-sided *t*-test. Error bars represent s.d.

Reporting Summary. Further information on research design is available in the Nature Research Reporting Summary linked to this article.

Data availability

References

43. Purcell, S. et al. PLINK: a tool set for whole-genome association and population-based linkage analyses. *Am. J. Hum. Genet.* **81**, 559–575 (2007).
44. Hinrichs, A. S. et al. The UCSC Genome Browser Database: update 2006. *Nucleic Acids Res.* **34**, D590–D598 (2006).
45. Sherry, S. T. et al. dbSNP: the NCBI database of genetic variation. *Nucleic Acids Res.* **29**, 308–311 (2001).
46. Browning, B. L. & Browning, S. R. Genotype imputation with millions of reference samples. *Am. J. Hum. Genet.* **98**, 116–126 (2016).
47. Loh, P.-R. et al. Reference-based phasing using the Haplotype Reference Consortium panel. *Nat. Genet.* **48**, 1443–1448 (2016).
48. Delaneau, O., Marchini, J. & Zagury, J.-F. A linear complexity phasing method for thousands of genomes. *Nat. Methods* **9**, 179–181 (2011).
49. Durbin, R. Efficient haplotype matching and storage using the positional Burrows–Wheeler transform (PBWT). *Bioinformatics* **30**, 1266–1272 (2014).
50. Fuchsberger, C., Abecasis, G. R. & Hinds, D. A. minimac2: faster genotype imputation. *Bioinformatics* **31**, 782–784 (2015).
51. Li, H. & Durbin, R. Fast and accurate short read alignment with Burrows–Wheeler transform. *Bioinformatics* **25**, 1754–1760 (2009).
52. Van der Auwera, G. A. et al. From FastQ data to high confidence variant calls: the Genome Analysis Toolkit best practices pipeline. *Curr. Protoc. Bioinformatics.* **43**, 11.10.1–11.10.33 (2013).
53. Powell, J. E., Visscher, P. M. & Goddard, M. E. Reconciling the analysis of IBD and IBS in complex trait studies. *Nat. Rev. Genet.* **11**, 800–805 (2010).
54. Zhernakova, D. V. et al. Identification of context-dependent expression quantitative trait loci in whole blood. *Nat. Genet.* **49**, 139–145 (2016).
55. Raj, T. et al. Polarization of the effects of autoimmune and neurodegenerative risk alleles in leukocytes. *Science* **344**, 519–523 (2014).
56. Yang, J., Fritsche, L. G., Zhou, X. & Abecasis, G. A scalable Bayesian method for integrating functional information in genome-wide association studies. *Am. J. Hum. Genet.* **101**, 404–416 (2017).
57. Lonsdale, J. et al. The Genotype–Tissue Expression (GTEx) project. *Nat. Genet.* **45**, 580–585 (2013).
58. Sun, B. B. et al. Genomic atlas of the human plasma proteome. *Nature* **558**, 73–79 (2018).
59. Ernst, J. & Kellis, M. ChromHMM: automating chromatin-state discovery and characterization. *Nat. Methods* **9**, 215–216 (2012).
60. Roadmap Epigenomics Consortium et al. Integrative analysis of 111 reference human epigenomes. *Nature* **518**, 317–330 (2015).
61. Ward, L. D. & Kellis, M. HaploRegv4: systematic mining of putative causal variants, cell types, regulators and target genes for human complex traits and disease. *Nucleic Acids Res.* **44**, D877–D881 (2016).
62. Bernstein, B. E. et al. An integrated encyclopedia of DNA elements in the human genome. *Nature* **489**, 57–74 (2012).
63. Heinz, S. et al. Simple combinations of lineage-determining transcription factors prime *cis*-regulatory elements required for macrophage and B cell identities. *Mol. Cell* **38**, 576–589 (2010).
64. Buenrostro, J. D., Giresi, P. G., Zaba, L. C., Chang, H. Y. & Greenleaf, W. J. Transposition of native chromatin for fast and sensitive epigenomic profiling of open chromatin, DNA-binding proteins and nucleosome position. *Nat. Methods* **10**, 1213–1218 (2013).
65. Zhang, Y. et al. Model-based analysis of ChIP-Seq (MACS). *Genome Biol.* **9**, R137 (2008).

nature research

Corresponding author(s):   Soumya Raychaudhuri

Reporting Summary

Nature Research wishes to improve the reproducibility of the work that we publish. This form provides structure for consistency and transparency in reporting. For further information on Nature Research policies, see Authors & Referees and the Editorial Policy Checklist.

Statistical parameters

When statistical analyses are reported, confirm that the following items are present in the relevant location (e.g. figure legend, table legend, main text, or Methods section).

n/a	Confirmed	
☐	☒	The exact sample size (*n*) for each experimental group/condition, given as a discrete number and unit of measurement
☐	☒	An indication of whether measurements were taken from distinct samples or whether the same sample was measured repeatedly
☐	☒	The statistical test(s) used AND whether they are one- or two-sided *Only common tests should be described solely by name; describe more complex techniques in the Methods section.*
☐	☒	A description of all covariates tested
☐	☒	A description of any assumptions or corrections, such as tests of normality and adjustment for multiple comparisons
☐	☒	A full description of the statistics including central tendency (e.g. means) or other basic estimates (e.g. regression coefficient) AND variation (e.g. standard deviation) or associated estimates of uncertainty (e.g. confidence intervals)
☐	☒	For null hypothesis testing, the test statistic (e.g. F, t, r) with confidence intervals, effect sizes, degrees of freedom and P value noted *Give P values as exact values whenever suitable.*
☐	☒	For Bayesian analysis, information on the choice of priors and Markov chain Monte Carlo settings
☐	☒	For hierarchical and complex designs, identification of the appropriate level for tests and full reporting of outcomes
☐	☒	Estimates of effect sizes (e.g. Cohen's d, Pearson's r), indicating how they were calculated
☐	☒	Clearly defined error bars *State explicitly what error bars represent (e.g. SD, SE, CI)*

Our web collection on statistics for biologists may be useful.

Software and code

Policy information about availability of computer code

Data collection	No software was used.
Data analysis	Plink 1.9, Beagle v4.1 (version 22Apr16.1cf), UCSC LiftOver, EAGLE v2.3.4, SHAPEIT v2.r837, PBWT v3.0, BWA-mem 0.7.12, PICARD 1.128, GATK v3.4, MACS v2.1.0, FINEMAP v1.1, Trinculo v0.96, Custom code is available at github (https://github.com/immunogenomics/ harmjan/tree/master/FinemappingPaper and https://github.com/immunogenomics/harmjan/tree/master/FinemappingTools)

For manuscripts utilizing custom algorithms or software that are central to the research but not yet described in published literature, software must be made available to editors/reviewers upon request. We strongly encourage code deposition in a community repository (e.g. GitHub). See the Nature Research guidelines for submitting code & software for further information.

Data

Policy information about availability of data

All manuscripts must include a data availability statement. This statement should provide the following information, where applicable:

- Accession codes, unique identifiers, or web links for publicly available datasets
- A list of figures that have associated raw data
- A description of any restrictions on data availability

All unique materials are readily available from the authors or the T1DGCC and RACI consortia. ATAC-seq data available as accession GSE116497 in NCBI Gene

Field-specific reporting

Please select the best fit for your research. If you are not sure, read the appropriate sections before making your selection.

☒ Life sciences ☐ Behavioural & social sciences ☐ Ecological, evolutionary & environmental sciences

For a reference copy of the document with all sections, see nature.com/authors/policies/ReportingSummary-flat.pdf

Life sciences study design

All studies must disclose on these points even when the disclosure is negative.

Sample size	We used logistic regression. Our study included 20,445 individuals for T1D, and 27,345 individuals for RA. Following Peduzzi et al., 1996, if we use the formula N = 10 k / p, where N represents the minimal number of individuals, k represents the number of covariates, and p the smallest proportion of individuals, we observe the following: considering a minor allele frequency of 1%, and considering 14 included covariates, the minimal sample size would be 14,000. Similarly, for RA, considering 16 covariates, the minimal sample size would be 16,000.
Data exclusions	Related samples were replaced by pseudo-controls in the T1D dataset, in order to account for inflation of allele frequencies due to relatedness. When merging overlapping controls in the RA and T1D dataset, we used genetic relatedness to remove overlapping controls.
Replication	EMSAs were replicated using titrations of either biotinylated probes or nuclear extract. Luciferase assays were performed using three independent transfections. All reported experimental results were successfully replicated.
Randomization	The study was not a clinical trial or interventional study. Hence there was no blinding or randomization that is applicable.
Blinding	The study was not a clinical trial or interventional study. Hence there was no blinding or randomization that is applicable.

Reporting for specific materials, systems and methods

Materials & experimental systems

n/a	Involved in the study
☐	☒ Unique biological materials
☒	☐ Antibodies
☐	☒ Eukaryotic cell lines
☒	☐ Palaeontology
☒	☐ Animals and other organisms
☐	☒ Human research participants

Methods

n/a	Involved in the study
☒	☐ ChIP-seq
☒	☐ Flow cytometry
☒	☐ MRI-based neuroimaging

Unique biological materials

Policy information about availability of materials

Obtaining unique materials	All unique materials are readily available from the autors or the T1DGCC and RACI consortia. ATAC-seq data available as accession GSE116497 in NCBI Gene expression omnibus.

Eukaryotic cell lines

Policy information about cell lines

Cell line source(s)	Jurkat and THP-1 cells, obtained from ATCC (TIB-152 and TIB-202)
Authentication	According to the ATCC: ATCC (https://www.atcc.org/~/media/PDFs/Technical%20Bulletins/tb08.ashx): "As a biological resource center, ATCC and other recognized cell banks comprehensively perform authentication and quality-control tests on all distribution lots of cell lines. Therefore, obtaining and using low-passage cell lines from ATCC is a sure way to work

and publish with confidence". Morphology of the cells was checked by microscope and the cells grew at a stable proliferation ratio.

Mycoplasma contamination	Since the cells were low passage and recently bought, they were not tested for mycoplasma contamination.
Commonly misidentified lines (See ICLAC register)	None of these cells are listed in the last version (8.0) of the commonly misidentified cell lines maintained by ICLAC.

Human research participants

Policy information about studies involving human research participants

Population characteristics	In this study we did not adjust for age and gender, but did adjust for genotype PCs, regional covariates and cohort, when needed. Covariate-relevant population characteristics are described in the respective studies describing the collection and recruitment of the RA and T1D cases and controls. These study designs are described here: Eyre et al, Nat. Genet., 2012, Onengut-Gumuscu, Nat. Genet., 2015
Recruitment	Participants were not recruited by the authors of this study.